

Human-Like Coarse Object Representations in Vision Models

Andrey Gizdov^{1,2*} Andrea Procopio^{1,3*} Yichen Li¹ Daniel Harari² Tomer Ullman¹

¹Harvard University ²Weizmann Institute of Science ³Bocconi University

{andreygizdov, aprocopio, yichenli, tullman}@fas.harvard.edu hararid@weizmann.ac.il

Abstract

Humans appear to represent objects for intuitive physics with coarse, volumetric “bodies” that smooth concavities – trading fine visual details for efficient physical predictions – yet their internal structure is largely unknown. Segmentation models, in contrast, optimize pixel-accurate masks that may misalign with such bodies. We ask whether and when these models nonetheless acquire human-like bodies. Using a time-to-collision (TTC) behavioral paradigm, we introduce a comparison pipeline and alignment metric, then vary model training time, size, and effective capacity via pruning. Across all manipulations, alignment with human behavior follows an inverse U-shaped curve: small/briefly trained/pruned models under-segment into blobs; large/fully trained models over-segment with boundary wiggles; and an intermediate “ideal body granularity” best matches humans. This suggests human-like coarse bodies emerge from resource constraints rather than bespoke biases, and points to simple knobs – early checkpoints, modest architectures, light pruning – for eliciting physics-efficient representations. We situate these results within resource-rational accounts balancing recognition detail against physical affordances.

1. Introduction

Human perception is concerned with *what* entities are present, *where* the entities are, and *how* a scene will unfold [14, 26]. The problems of ‘what’, ‘where’, and ‘how’ are coupled but separate, and it is likely that they are supported by computations and representations that are coupled but separate. In particular, for the purposes of inferring the *identity* of objects (e.g. telling apart a thermos and a water bottle) it may be important to have fine-grain object segmentation, but for the purposes of estimating *how* a physical scene will unfold (which objects will collide, and where they will end up), it may be sufficient and more cost-effective to have more coarse object-representations (e.g. if

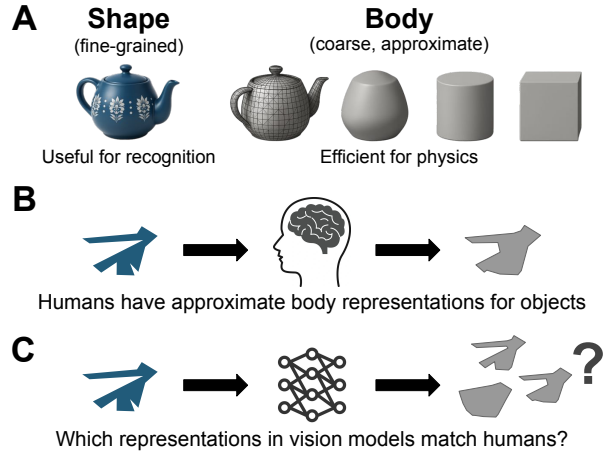


Figure 1. **Research overview.** (A) Different object representations are useful for different goals. “Body” representation is useful for physical reasoning. “Shape” representation is useful for recognition. (B) Prior work [25] has shown evidence that humans do have such coarse body representations for physical reasoning (e.g. predicting collision times), specifically by “filling in” concave regions. (C) Our research asks *whether* vision segmentation models have such similar representations and under *what* conditions they develop them.

all that matters is catching or ducking them up, a water bottle and thermos can be roughly approximated by a cylinder). The separation between coarse and fine-grain object representations for different purposes is widely used in engineering, especially in simulated environments such as games and animations. Computational models of intuitive physics in humans suggest people may have a similar split between physics and graphics [4, 46], with fine-grain object *shapes* used for rendering and recognition, and coarse-grain *body* representations used for physical prediction and action (see Figure 1A). This suggestion is in line with studies that show infants first carve the visual field into cohesive but rough volumetric entities with approximate spatial extent, before they infer contact relations, support, or motion trajectories [2, 43]. Recent psychophysical studies with adults also suggest that humans use coarse body approximations [25]

*Equal contribution.

(see Figure 1B). In particular, there’s evidence that people’s body approximations tend to “fill in” concave object regions (“*Related work*” and Section 3.1 discuss this in detail). From a neuro-scientific perspective, the physics/graphics split may map onto the neural division between the dorsal and ventral streams in human vision [4].

While evidence suggests humans rely on approximate representations of objects when reasoning about physics, the nature and structure of these representations in the human brain remain largely unknown. Behavioral methods offer indirect, low-resolution glimpses into these internal encodings, and do not reveal their geometric or computational form. Artificial segmentation models, which are trained to perform a similar decomposition of scenes into discrete entities, offer in principle a natural computational proxy for exploring how such representations might form in the human brain. If modern vision models trained for segmentation or prediction share representational structure with humans, they could provide a scalable way of revealing the coarse object representations that support intuitive physics and action.

However, in nearly all segmentation models and datasets where an explicit teaching signal, reward, or loss function is used, the target is ground-truth segmentation or pixel-perfect human annotation. Such fine-grained segmentation may be useful for object recognition, but it may *diverge* from the approximate object representations that underpin human physical intuition. This misalignment is both inefficient and risky: fine-grain representations waste computation and can lead AI agents to mis-predict human behavior, since people act based on intuitive, coarse-grain physics rather than exact geometry. *Unlike* the study of alignment in LLMs, there has been relatively little exploration of the alignment between the body representations humans use when reasoning about physics and the object representations machine models use for vision, which are often used as a basis for downstream physics tasks. Given that (i) coarse object bodies are useful for physical simulations in engineered systems, (ii) humans appear to rely on coarse bodies during physical reasoning, and (iii) segmentation networks can learn such abstractions, we ask the following question (Figure 1C): *Do segmentation models form object representations that match those observed in humans during physical reasoning?*

In this study, we create a pipeline for such comparison and explicitly control three key factors: model size, training time, and active neuron count (via unstructured pruning). As such, aside from answering the question of *whether* vision models and humans share similar representations, we attempt to answer the question *why: under what mechanistic conditions do such similarities emerge?*

Contributions. Our contributions are as follows:

1. **A general pipeline for comparing segmentation mod-**

els with human physical judgments. We operationalize coarse “body” representations in segmentation networks and introduce a unified Time-To-Collision (TTC) evaluation framework using data from 226 human participants [25]. This framework enables direct, quantitative comparison between vision model predictions and human behavior (see Section 3).

2. **We find a *U-shaped* relationship between segmentation detail and error relative to humans.** Across six transformer-based segmentation networks of the same family, error with respect to human TTC judgments is not monotonic in segmentation quality: very small or heavily pruned models under-segment objects into overly coarse blobs, while very large, fully trained models over-segment with pixel-perfect masks. Both extremes yield higher human–model disagreement, whereas error is minimized at an intermediate regime of “ideal” segmentation granularity (see Section 4).
3. **This *U-shaped* error reliably appears as a function of model size, training steps, and effective neural capacity.** We show this coarse → ideal → over-detailed pattern as a function of three parameters: (i) model size, (ii) training steps, and (iii) effective neural capacity (via unstructured pruning). In all cases, human–model error forms a U-shaped curve: highest at small and large values of the parameters, and lowest at an intermediate regime (see Section 4.1, 4.2, 4.3).
4. **We provide a computational account of why humans may use coarse body representations for intuitive physics.** Across these manipulations, human-like bodies are most prominent near the ideal segmentation granularity regime, where representational and computational resources are limited but not extreme. This suggests that similar coarse encodings in biology may arise as an efficient compromise under constraints on brain size, neural capacity, and metabolic cost, rather than a species-specific characteristic (see Section 5).

Our results provide practical and theoretical insight. Practically, understanding when models form human-like object bodies is important for designing vision systems that interact safely and predictably with humans. Theoretically, we identify computational conditions under which human-like body representations emerge, offering a mechanistic account of why humans may simplify object geometry during intuitive physical reasoning.

2. Related Work

People reason efficiently about everyday physical dynamics, though they show systematic biases under certain conditions [19, 22]. This “intuitive physics” emerges early [3, 44], is supported by dedicated neural systems [5, 11, 31, 32], and is likely shared with non-human animals [42, 48].

There are different competing formal accounts of the men-

tal computations that support intuitive physics. One currently prominent view suggests that people mentally simulate physical events, somewhat like the game engines or physics engine used to simulate fictional worlds in computer games and animation [8, 20, 46]. The mental-game-engine proposal has been used to investigate and explain people’s reasoning about a variety of physical phenomena, including collisions, stability, tool use, liquids, rigid- and soft-body motion, physical prediction, and physical counterfactuals and causal reasoning [7–9, 15, 18, 35, 39–41].

Prior to, and proceeding alongside the mental simulation account, a variety of non-simulation accounts of intuitive physics have also been proposed. These include, but are not limited to, the use of heuristics, logical rules, bottom-up visual features, qualitative reasoning, and pre-Newtonian theory-like abstractions [1, 10, 12, 13, 16, 24, 27–30, 33, 37]. Some of these accounts point to people’s errors as evidence that humans cannot be running a perfect simulation, as such a simulation would be too costly and not make errors. However, if such a mental simulation exists in the mind, it cannot be perfectly accurate. Just as engineered simulations make heavy use of various approximations and workarounds, it is likely that people’s mental simulation uses approximations as well [4, 6, 46, 47].

One major approximation in simulated environments is the use of simplified objects for the purposes of physical tracking and collision handling. While an advanced game engine may use fine-grain meshes to graphically render high-resolution images, it will often use only rough bodies for the purposes of collision detection and physics simulation. Converging theoretical and empirical work suggests that humans similarly use approximate “body” representations in physical reasoning [25, 46] – volumetric approximations that prioritize properties relevant to action and physical interaction (e.g., mass, position, and rough form) while discarding fine-grained visual details (Figure 1 A, B). This idea is consistent with resource-rational accounts of cognition, and the “what/where–how” functional split in visual processing.

In this paper, we focus on the Time-To-Collision experiment from Li et al. [25], in which participants watched an agent object move toward a patient object, and were asked to press a key when they predicted the two objects would collide (Figure 2A, more details in Section 3.1). This experiment is in turn based on a well-established paradigm that investigates people’s time-to-collision judgments with simple bodies [17, 34, 45]. A key behavioral signature is an asymmetry between *concave* and *convex* stimuli: Different from what a random noise model would predict, human judgments seem to selectively smooth or “fill in” concavities on objects (over-approximating inlets and gaps), predicting earlier collision for concave than convex pairings. Preliminary analyses suggested that the operative body rep-

resentation is between the exact outline and the convex hull. Segmentation networks are natural probes of object form, because they decompose scenes into entities prior to downstream inference. Yet most of these models are trained for pixel-accurate boundaries, favoring fine detail that may be misaligned with human physical prediction. Prior work has leveraged coarse bodies for modeling human expectations without direct comparison to people [38], or has used α -shape-based models to analyze human approximations without endorsing them as cognitive mechanisms [25], but as a way of teasing apart different degrees of approximation. Aside from offering glimpses into potential parallels between human and model representations, our work takes a more detailed view of how such representations evolve during training. Rather than focusing on global alignment metrics, we investigate the micro-level dynamics of segmentation learning—how sensitivity to different geometric structures, particularly concavities, changes as models grow or train longer. This approach complements broader forecasting efforts that aggregate model performance as a function of scale or time [21, 23, 36], by revealing the finer representational shifts that underlie those macro-level trends.

3. Methods

Here we outline how we compare vision models with human behavior in the Time-To-Collision (TTC) experiment. The human behavioral data was acquired from Li et al. [25]. This dataset is *not* the contribution of this work; we only *use* this data. We detail in this section our fine-tuning pipeline for the vision models, and how we map the vision model’s response to human behavior.

3.1. Human dataset

The dataset given to 226 human participants [25] consists of 96 videos of 2 objects, one moving towards the other. At a certain point in time (the ground truth TTC), the stationary object becomes invisible and participants are asked to press a button when they think the two have collided (see Figure 2A). Humans react significantly earlier when one of the objects has its concave side facing the collision (suggesting that humans *literally* “fill in concavities” mentally). The dataset provides a TTC recording from each participant for each video.

3.2. Vision models

Architectures. To adapt vision models to the same task, we use six versions of the publicly available SegFormer model: a hierarchical transformer encoder with a lightweight MLP decoder. The versions we use only vary in parameter count, from $\sim 3.8M$ (B0) to $\sim 84.7M$ (B5), but follow the same architecture (see Supplementary, section “*Model architectures*”). The ADE20K dataset contains everyday scenes; we use public SegFormer checkpoints [49] pretrained on

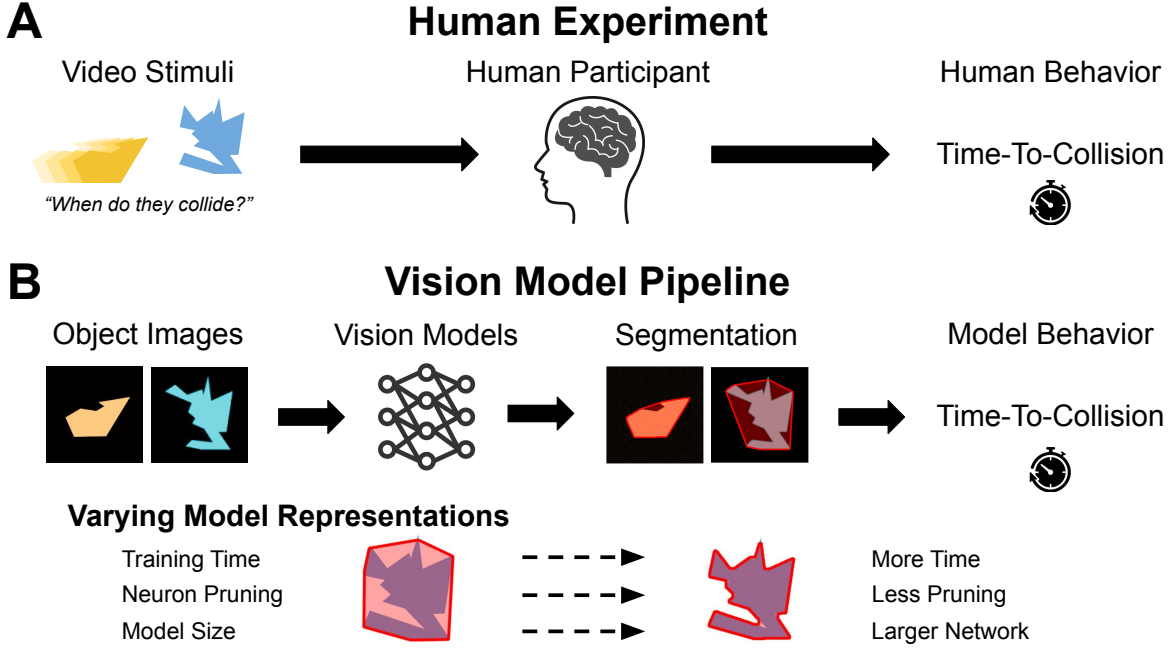


Figure 2. Method: We compared human behavioral responses with vision model’s responses in a time-to-collision task. (A) In prior work, human participants watched short videos showing objects moving towards one another, and were asked to respond as soon as they predicted the collision happened. Time-to-collision (TTC) response were collected from humans, which showed a systematic pattern that object pairs with collision points inside a concavity seemed to collide sooner than they actually were – an effect of “filling in” concavities on an object due to coarse body approximation. **(B)** In this paper, we take pre-trained segmentation models to perform the same task and compare each model’s TTC responses with humans. We systematically varied different aspects of training to adjust the coarseness of object representations in vision models.

ADE20K to provide broad visual priors [50]. Across B0–B5, the encoder depth (blocks per stage), embedding dimensions, and attention heads scale up monotonically, while the lightweight MLP decoder is kept fixed; no other architectural changes are introduced.

Fine-tuning paradigm. The models we use are purely for segmentation. Before we describe how we go from *segmentations* to *TTC*, we briefly explain how the models are fine-tuned. Models pre-trained on real-world datasets (such as ADE20K [50]) do not reliably segment the novel polygonal stimuli used in the human experiments (see Figure 2B). Therefore, we fine-tune each model on a synthetic dataset created by us (see below), designed to approximate the geometric statistics and scene structure of the human stimuli. For fine-tuning, we use the following hyperparameters: AdamW optimizer with learning rate 5×10^{-5} , cosine learning rate schedule with warmup, batch size of 4, weight decay of 0.01, and 10 epochs, or 1250 training steps. The training was performed on NVIDIA A100 GPUs with mixed precision (bfloating16) and TF32 optimizations enabled. The models are trained with a combination of cross-entropy and Dice loss to segment the binary segmentation task.

Synthetic dataset. We generate **500** training images, and

200 validation images; no shape is shared across splits and we never fine-tune on any frame from the human stimuli videos. Each training image contains a single uniformly colored polygon on a black background, making our model more accustomed to the data shown to humans. We developed a procedural polygon generator to produce geometrically diverse yet controlled stimuli. Each polygon is created by sampling: (1) a vertex count uniformly from 5–12; (2) a number of concavities (0–3); and (3) irregularity and spikiness parameters controlling local curvature and edge variance. Polygons are rendered on black backgrounds using one of 24 bright colors sampled from a palette matched to the luminance distribution of the experimental stimuli. The generator thus produces a broad range of shapes that maintain the key structural properties of the human-tested stimuli while preventing any overlap between training and evaluation data. The dataset will be released publicly upon paper acceptance.

3.3. From segmentation masks to TTC

Once trained, we test the models on the same videos shown to humans. Each video depicts two objects that would collide after a known ground-truth time-to-collision TTC_{gt}

if both remained visible and continued moving (see Section 3.1, [25]). Before motion starts, both objects are stationary and fully visible. We extract this initial static frame

$$I \in \mathbb{R}^{H \times W \times 3},$$

in which both objects are present and no motion has yet occurred. Our segmentation models are trained as binary segmenters with two classes: background (class 0) and object (class 1). Given I , the model outputs per-pixel logits

$$\mathbf{L}(I) \in \mathbb{R}^{H \times W \times 2}.$$

We apply a softmax over the class dimension and take an argmax to obtain a single foreground mask that contains *both* objects:

$$\mathbf{M}(I) = \mathbf{1} \left[\arg \max_{c \in \{0,1\}} \text{softmax}(\mathbf{L}(I))_c = 1 \right] \in \{0,1\}^{H \times W},$$

where pixels labeled 1 are predicted as “object” and pixels labeled 0 as “background”. We then extract the two largest connected components of $\mathbf{M}(I)$ and denote them by

$$\mathbf{M}_1, \mathbf{M}_2 \in \{0,1\}^{H \times W},$$

corresponding to the two segmented objects in the scene. From the data of Li et al. [25] we know the true velocities of the two objects in image coordinates,

$$\mathbf{v}_1, \mathbf{v}_2 \in \mathbb{R}^2$$

(in pixels per frame), as well as the frame rate Δf (frames per second). We define a translation operator

$$\text{Translate}(\mathbf{M}, \mathbf{u})$$

that shifts a binary mask \mathbf{M} by a displacement vector \mathbf{u} in the image plane. We then simulate the future motion of the two segmented objects using only their initial masks and the true velocities. At discrete frame index $n \in \mathbb{N}$, the translated masks are

$$\mathbf{M}_1^{(n)} = \text{Translate}(\mathbf{M}_1, n\mathbf{v}_1),$$

$$\mathbf{M}_2^{(n)} = \text{Translate}(\mathbf{M}_2, n\mathbf{v}_2).$$

The model-predicted time-to-collision (TTC) for that video is the earliest time $t = \frac{n}{\Delta f}$ (in seconds) at which the translated masks first overlap:

$$\text{TTC}_{\text{model}} = \min_{n \geq 0} \left\{ t = \frac{n}{\Delta f} \mid \mathbf{M}_1^{(n)} \cap \mathbf{M}_2^{(n)} \neq \emptyset \right\}.$$

In this way, the model receives the same static pre-motion frame as the human observer and uses only its inferred object masks, together with the true kinematics of the original stimuli, to produce a TTC prediction.

3.4. Comparing model and human behavior

The human dataset contains videos with different ground-truth times-to-collision TTC_{gt} and different shape configurations. For each TTC_{gt} , there are matched pairs of videos in which either a concave side of one object faces the collision or a convex side faces the collision. Crucially, these concave and convex videos share the same kinematics and ground-truth collision time; the only difference is the local shape facing the impact.

For each video n and participant p , we observe a human response time $\text{TTC}_{\text{human}}^{(n,p)}$, defined as the time between motion onset and the button press. We first average across participants to obtain a per-video human TTC,

$$\text{TTC}_{\text{human}}^{(n)} = \frac{1}{P} \sum_{p=1}^P \text{TTC}_{\text{human}}^{(n,p)}.$$

We index videos by their ground-truth collision time τ and shape condition $g \in \{\text{concave}, \text{convex}\}$. Let $\mathcal{N}(\tau, g)$ be the set of videos with $\text{TTC}_{\text{gt}} = \tau$ and condition g . We define the condition-averaged human TTC as

$$\text{TTC}_{\text{human}}(\tau, g) = \frac{1}{|\mathcal{N}(\tau, g)|} \sum_{n \in \mathcal{N}(\tau, g)} \text{TTC}_{\text{human}}^{(n)}.$$

The human concavity effect at ground-truth time τ is then

$$\Delta_{\text{human}}(\tau) = \text{TTC}_{\text{human}}(\tau, \text{concave}) - \text{TTC}_{\text{human}}(\tau, \text{convex}),$$

which measures how much earlier (or later) people respond when a concave side faces the collision, holding the true TTC and kinematics fixed.

We compute an analogous quantity for the model. For each video n we obtain $\text{TTC}_{\text{model}}^{(n)}$ via the segmentation-based simulation above. We then average over videos with the same (τ, g) :

$$\text{TTC}_{\text{model}}(\tau, g) = \frac{1}{|\mathcal{N}(\tau, g)|} \sum_{n \in \mathcal{N}(\tau, g)} \text{TTC}_{\text{model}}^{(n)},$$

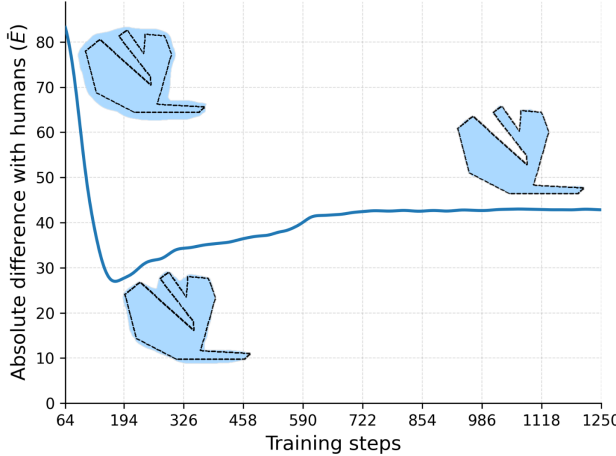
and define the model concavity effect

$$\Delta_{\text{model}}(\tau) = \text{TTC}_{\text{model}}(\tau, \text{concave}) - \text{TTC}_{\text{model}}(\tau, \text{convex}).$$

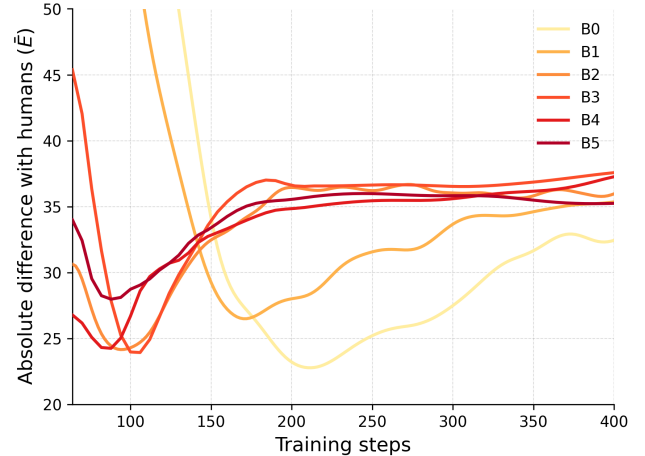
Our primary alignment metric for a given ground-truth time τ is the absolute difference between human and model concavity effects:

$$E(\tau) = |\Delta_{\text{model}}(\tau) - \Delta_{\text{human}}(\tau)|.$$

We report $E(\tau)$ as a function of training time, model size, and pruning level, and also aggregate across τ where appropriate by averaging $E(\tau)$ over all ground-truth TTCs. Because concave and convex videos share the same



(a) Difference between model and human behavior across training steps.



(b) Comparison of different model sizes.

Figure 3. Effect of training time on the difference between model behavior and human behavior. (a) Moderately approximate body representation emerges from medium training time, and aligns best with human behavior. Y-axis shows the difference between model and human responses \bar{E} . 3 example visualizations of the segmentation mask along training time are shown, from the most coarse (beginning of training), to intermediate coarse (after short training), to very fine-grained (end of training). (b) Larger models require less training time to reach the most human-like body representation. Larger models (e.g. B2-B5) converge to the point with the smallest difference to human behavior faster than smaller models (B0, B1).

ground-truth TTC and velocities, any systematic difference $\Delta_{\text{model}}(\tau)$ arises from how the model represents objects in those regions (e.g., “filling in” concavities vs. preserving them). *Importantly*, we are not measuring global segmentation coarseness, but the *differential* treatment of concave vs. convex regions under matched physical conditions.

4. Results

We report the results on the TTC experiment, comparing model behavior with human behavior using the concavity effect metric $\Delta_{\text{model}}(\tau)$ and its deviation from the human effect $\Delta_{\text{human}}(\tau)$. For each model setting, we summarize performance by the average absolute error

$$\bar{E} = \frac{1}{|\mathcal{T}|} \sum_{\tau \in \mathcal{T}} |\Delta_{\text{model}}(\tau) - \Delta_{\text{human}}(\tau)|,$$

where \mathcal{T} indexes all ground-truth TTC values. Lower \bar{E} indicates that the model’s concave–convex difference more closely matches humans’ concave–convex differences.

We systematically vary three factors that change the model’s effective capacity and, by extension, its object representations: (i) training time, (ii) model size, and (iii) pruning strength. In all three cases, we observe a consistent U-shaped pattern: \bar{E} is high for very low and very high capacity, and is minimized at an intermediate regime. We refer to this intermediate regime as the “ideal body granularity” regime, where object bodies are neither too coarse nor too over-detailed, and the concavity effect best matches human

behavior. *Importantly*, our analysis targets this concave-convex difference rather than generic segmentation coarseness, which has been studied extensively before.

4.1. Training time

For each SegFormer variant, we save checkpoints at regular intervals along training and compute \bar{E} at each checkpoint. Intuitively, early in training the model has only a crude grasp of object extent, while late in training it converges to highly precise, boundary-optimized segmentations. Indeed, this can be seen visualized in the overlaid representations in Figure 3. Here, we study how that precision differs for concave-convex object regions compared to humans.

Figure 3 shows \bar{E} as a function of training steps for a representative model. The *first* finding here is that segmentation models do diffuse concave body parts more than convex body parts, which was not clear a priori. It is known that coarseness converges and reduces during training, but apparently, the velocity of *convergence*, as indicated by the non-zero value of \bar{E} , is different for concave and convex object parts (see Figure 6). Secondly, the error is large at the very beginning of training, then decreases and reaches a minimum at an intermediate number of updates, before rising again as the model continues to optimize for pixel-accurate segmentation.

4.2. Pruning of neurons

Pruning changes the model’s effective capacity at inference time without retraining. Starting from a trained model, we

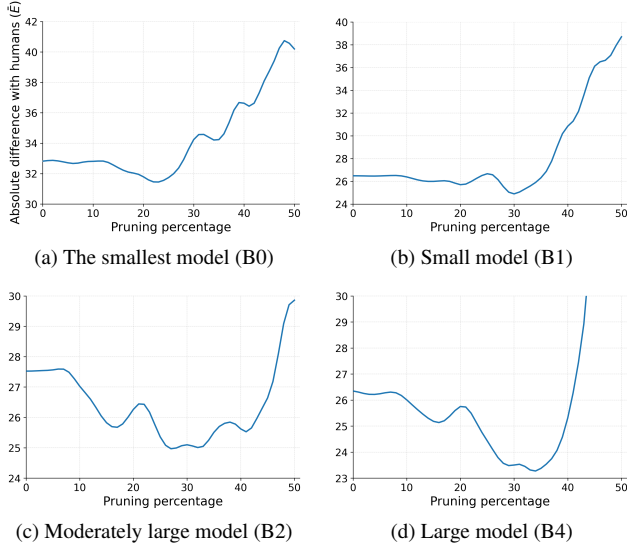


Figure 4. Moderate pruning of neurons produces more human-like body representations. The x-axis shows the strength of pruning (i.e. percentage of neurons removed). The y-axis shows the difference between model behavior and human behavior \bar{E} .

perform magnitude-based pruning: for each pruning level, we rank weights by absolute value and set the smallest-magnitude weights to zero, effectively silencing the corresponding neurons. We sweep over pruning fractions and recompute \bar{E} at each level.

As shown in Figure 4, \bar{E} again follows a U-shaped curve as a function of pruning strength. With no pruning, the model produces overly fine, fragmented masks; with very strong pruning, it collapses to coarse blobs and loses the concavity effect. Intermediate pruning levels yield the lowest error, indicating that human-like concave–convex differences arise at an intermediate effective capacity. This supports the view that the ideal body granularity regime reflects a general constraint on available representational bandwidth *at inference time*, in addition to a property of training dynamics.

4.3. Model size

Finally, we vary the model size directly. We test six SegFormer variants (B0–B5) spanning parameter counts from $\sim 3.8\text{M}$ (B0) to $\sim 84.7\text{M}$ (B5), thus covering over an order of magnitude in capacity. All models are trained with the same objective and dataset, and we evaluate \bar{E} at convergence.

Figure 5 plots \bar{E} as a function of model size. The smallest models (e.g., B0) under-segment objects, producing very coarse bodies that fail to capture the concavity effect observed in humans. The largest models (e.g., B4–B5) over-segment, focusing on pixel-perfect boundaries and fine irregularities that again misalign with human TTC behavior. Intermediate-sized models (e.g., B1–B2) achieve the low-

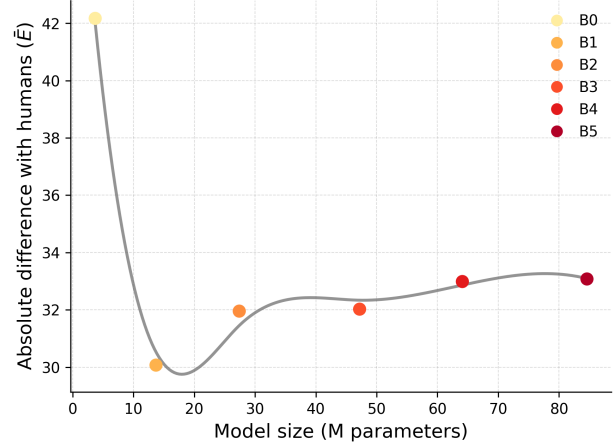


Figure 5. Models of intermediate sizes behave more human-like than small or large models, after a fixed number of training steps. The x-axis shows different model sizes. The y-axis shows the difference between model behavior and human behavior. Model size goes from small (B0) to large (B5).

est error, resulting in a concave–convex TTC shift that most closely matches human behavior.

4.4. Visual representation

For a visual intuition of the above results, we refer the reader to Figure 6. On the *top row*, segmented masks show clear outward diffusion around concavities, while corners and convex edges remain stable. The same pattern appears in the *bottom row* of probability maps, where activations spread beyond concave boundaries. This consistent “filling-in” effect suggests that models, like humans, simplify concave regions into smoother, coarser body representations. Taken together, the training-time, pruning, and model-size experiments all point to the same conclusion: human-like concavity effects in TTC arise most clearly at an intermediate, ideal body granularity. This regime is reached by different routes—mid-training checkpoints, intermediate pruning strengths, and mid-sized architectures—supporting the view that concave-convex differences emerge as a general consequence of a resource-constrained representations.

5. Discussion

People do not need pixel-accurate object representations to reason efficiently about everyday physical events. Instead, they rely on approximate “body” representations – coarse, volumetric encodings that preserve where mass is and how it can move, while discarding high-frequency details and textures. We asked whether analogous approximations arise in vision segmentation networks, and whether such “bodies” align with human behavior.

Across experiments, we observe systematic parallels be-

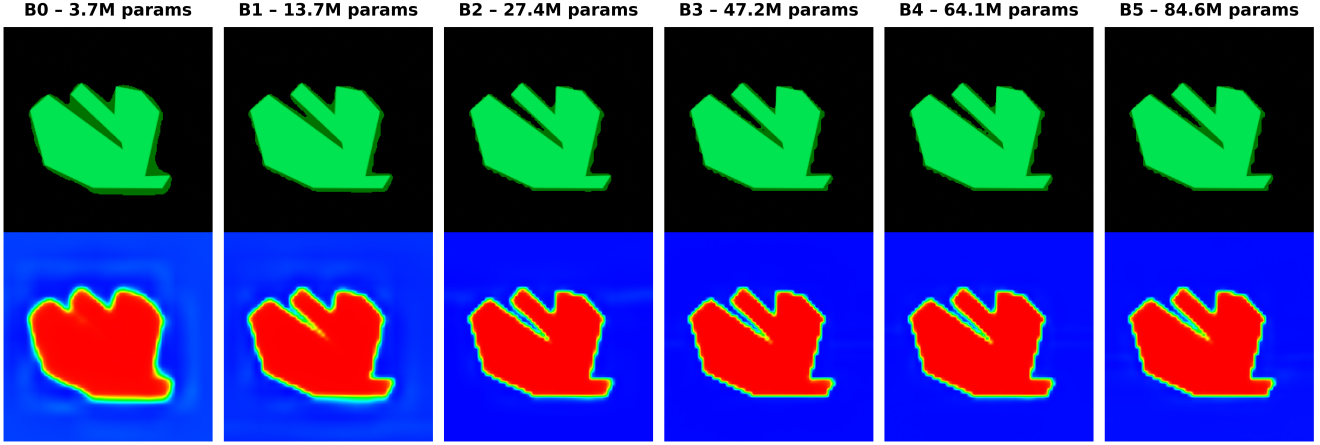


Figure 6. Mask overlays (first row) and probability heatmaps after 10 epochs of training across models. The training converges faster on convex object parts. See the Supplementary "Convergence speed" section for a quantitative account. The effect is observed for both model size and training time.

tween humans and vision models. Both simplify concavities – effectively “filling in” voids – while maintaining stable detail on convex parts. We show that (i) mid-training models produce moderately approximate bodies that best align with human judgments; (ii) larger models reach a human-like regime earlier in training; and (iii) light neuron pruning nudges networks toward more human-like bodies without bespoke objectives.

The effects that we found reasonably depend on resource budgets: Shorter training, smaller networks, and limited representational capacity emphasize low-frequency geometry and smooth over concavities; prolonged optimization and greater capacity sharpen boundaries and drift toward recognition-oriented detail. The human visual system has its own share of resource limitations, and develops under strict metabolic and informational constraints, time pressure, and limited perceptual resolution, which may bias it toward efficient, lower-complexity internal representations that emphasize overall object geometry and physical affordances. So, human-like approximate object representations can emerge from generic resource constraints rather than specialized inductive biases, and recognition accuracy and physics utility may occupy different points along a coarse-to-fine continuum.

Precise segmentation is indispensable for tasks that depend on exact contours, such as instance annotation or fine-grained recognition. But for physical reasoning, “not too fine, not too coarse” appears optimal: bodies that capture mass layout and physical affordances without overfitting boundary wiggles. Practically, this suggests simple knobs – early training snapshots, modest architectures, or gentle pruning – to elicit physics-efficient representations from standard models. Theoretically, resource-rational accounts of cognition predict this outcome: under the constraints of

limited bandwidth, time, and computation, both brains and machines converge on simplified internal encodings that trade fine detail for stable, predictive structure.

Our evaluation focused on time-to-collision, with a limited set of shapes, and a limited subset of architectures. We see several limitations and extensions: (i) Stimuli and tasks: move beyond 2D polygons to realistic 3D scenes; test additional psychophysics tasks beyond collision prediction. (ii) Model breadth: include diverse segmentation backbones, pretraining regimes, and models trained directly on dynamic videos. (iii) Mechanisms: probe causal levers (memory capacity, inference time complexity, representational sparsity, learning objectives) and quantify internal geometry (frequency content, convexity sensitivity) across training. (iv) Neuroscience links: connect to neurocomputational motifs (receptive-field pooling, task-dependent gating, representational sparsity) and evaluate alternative architectures (e.g., recurrent, energy-based, or dynamics-trained models) that may instantiate these mechanisms more directly.

In sum, coarse body representations are not a failure mode of segmentation. They are a useful operating point for physical reasoning. By showing when and how the alignment of such bodies with humans emerges in standard vision models, we offer a computational account of why humans simplify object structure in intuitive physics, and outline practical strategies to elicit similarly human-aligned representations in machine vision.

References

- [1] Renée Baillargeon. The acquisition of physical knowledge in infancy: A summary in eight lessons. *Blackwell handbook of childhood cognitive development*, pages 47–83, 2002. 3
- [2] Renée Baillargeon. Infants’ reasoning about hidden objects: Evidence for event-general and event-specific expectations. *Developmental Science*, 7(4):391–414, 2004. 1
- [3] Renée Baillargeon. Infants’ understanding of the physical world. In *Advances in Psychological Science, Volume 2*, pages 503–529. Psychology press, 2014. 2
- [4] Halely Balaban and Tomer D Ullman. Physics versus graphics as an organizing dichotomy in cognition. *Trends in Cognitive Sciences*, 2025. 1, 2, 3
- [5] Halely Balaban, Kevin A Smith, Joshua B Tenenbaum, and Tomer D Ullman. Electrophysiology reveals that intuitive physics guides visual tracking and working memory. *Open Mind*, 8:1425–1446, 2024. 2
- [6] Ilona Bass, Kevin A Smith, Elizabeth Bonawitz, and Tomer D Ullman. Partial mental simulation explains fallacies in physical reasoning. *Cognitive Neuropsychology*, 38 (7-8):413–424, 2021. 3
- [7] Christopher J Bates, İlker Yıldırım, Joshua B Tenenbaum, and Peter Battaglia. Modeling human intuitions about liquid flow with particle-based simulation. *PLoS computational biology*, 15(7):e1007210, 2019. 3
- [8] Peter W. Battaglia, Jessica B. Hamrick, and Joshua B. Tenenbaum. Simulation as an engine of physical scene understanding. *Proceedings of the National Academy of Sciences*, 110 (45):18327–18332, 2013. 3
- [9] Neil R Bramley, Tobias Gerstenberg, Joshua B Tenenbaum, and Todd M Gureckis. Intuitive experimentation in the physical world. *Cognitive psychology*, 105:9–38, 2018. 3
- [10] Ernest Davis. *Representations of commonsense knowledge*. Morgan Kaufmann, 1990. 3
- [11] Jason Fischer, John G Mikhael, Joshua B Tenenbaum, and Nancy Kanwisher. Functional neuroanatomy of intuitive physical inference. *Proceedings of the national academy of sciences*, 113(34):E5072–E5081, 2016. 2
- [12] Kenneth D Forbus. Qualitative physics: Past, present, and future. In *Exploring artificial intelligence*, pages 239–296. Elsevier, 1988. 3
- [13] Katerina Fragkiadaki, Pulkit Agrawal, Sergey Levine, and Jitendra Malik. Learning visual predictive models of physics for playing billiards. *arXiv preprint arXiv:1511.07404*, 2015. 3
- [14] Jennifer J Freyd. Dynamic mental representations. *Psychological review*, 94(4):427, 1987. 1
- [15] Tobias Gerstenberg and Simon Stephan. A counterfactual simulation model of causation by omission. *Cognition*, 216: 104842, 2021. 3
- [16] David L Gilden and Dennis R Proffitt. Understanding collision dynamics. *Journal of Experimental Psychology: Human Perception and Performance*, 15(2):372, 1989. 3
- [17] Rob Gray and Ian M Thornton. Exploring the link between time to collision and representational momentum. *Perception*, 30(8):1007–1022, 2001. 3
- [18] Jessica B Hamrick, Peter W Battaglia, Thomas L Griffiths, and Joshua B Tenenbaum. Inferring mass in complex scenes by mental simulation. *Cognition*, 157:61–76, 2016. 3
- [19] Joshua K Hartshorne and Mengguo Jing. Insights into cognitive mechanics from education, developmental psychology and cognitive science. *Nature Reviews Psychology*, pages 1–15, 2025. 2
- [20] Mary Hegarty. Mechanical reasoning by mental simulation. *Trends in cognitive sciences*, 8(6):280–285, 2004. 3
- [21] Joel Hestness, Sharan Narang, Newsha Ardalani, Gregory Diamos, Heewoo Jun, Hassan Kianinejad, Md. Mostofa Ali Patwary, Yang Yang, and Yanqi Zhou. Deep learning scaling is predictable, empirically, 2017. 3
- [22] James R Kubricht, Keith J Holyoak, and Hongjing Lu. Intuitive physics: Current research and controversies. *Trends in cognitive sciences*, 21(10):749–759, 2017. 2
- [23] Thomas Kwa, Ben West, Joel Becker, Amy Deng, Kathryn Garcia, Max Hasin, Sami Jawhar, Megan Kinniment, Nate Rush, Sydney Von Arx, Ryan Bloom, Thomas Broadley, Haoxing Du, Brian Goodrich, Nikola Jurkovic, Luke Harold Miles, Seraphina Nix, Tao Lin, Neev Parikh, David Rein, Lucas Jun Koba Sato, Hjalmar Wijk, Daniel M. Ziegler, Elizabeth Barnes, and Lawrence Chan. Measuring ai ability to complete long tasks, 2025. 3
- [24] Adam Lerer, Sam Gross, and Rob Fergus. Learning physical intuition of block towers by example. In *International conference on machine learning*, pages 430–438. PMLR, 2016. 3
- [25] Yichen Li, YingQiao Wang, Tal Boger, Kevin A. Smith, Samuel J. Gershman, and Tomer D. Ullman. An approximate representation of objects underlies physical reasoning. *Journal of Experimental Psychology: General*, 152(11):3074–3086, 2023. 1, 2, 3, 5
- [26] David Marr. *Vision: A computational investigation into the human representation and processing of visual information*. MIT press, 2010. 1
- [27] Michael McCloskey and Deborah Kohl. Naive physics: the curvilinear impetus principle and its role in interactions with moving objects. *Journal of Experimental Psychology: Learning, Memory, and Cognition*, 9(1):146, 1983. 3
- [28] Roozbeh Mottaghi, Hessam Bagherinezhad, Mohammad Rastegari, and Ali Farhadi. Newtonian scene understanding: Unfolding the dynamics of objects in static images. In *Proceedings of the IEEE Conference on Computer Vision and Pattern Recognition*, pages 3521–3529, 2016.
- [29] Manfred Nusseck, Julien Lagarde, Benoit Bardy, Roland Fleming, and Heinrich H Bülthoff. Perception and prediction of simple object interactions. In *Proceedings of the 4th Symposium on Applied Perception in Graphics and Visualization*, pages 27–34, 2007.
- [30] Luis S Piloto, Ari Weinstein, Peter Battaglia, and Matthew Botvinick. Intuitive physics learning in a deep-learning model inspired by developmental psychology. *Nature human behaviour*, 6(9):1257–1267, 2022. 3
- [31] RT Pramod, Michael A Cohen, Joshua B Tenenbaum, and Nancy Kanwisher. Invariant representation of physical stability in the human brain. *elife*, 11:e71736, 2022. 2

[32] RT Pramod, Elizabeth Mieczkowski, Cyn X Fang, Joshua B Tenenbaum, and Nancy Kanwisher. Decoding predicted future states from the brain’s “physics engine”. *Science Advances*, 11(22):eadr7429, 2025. 2

[33] Dennis R Proffitt, Mary K Kaiser, and Susan M Whelan. Understanding wheel dynamics. *Cognitive psychology*, 22(3): 342–373, 1990. 3

[34] David A Rosenbaum. Perception and extrapolation of velocity and acceleration. *Journal of Experimental Psychology: Human Perception and Performance*, 1(4):395, 1975. 3

[35] AN Sanborn, VK Mansinghka, and TL Griffiths. Reconciling intuitive physics and newtonian mechanics for colliding objects. *Psychological Review*, 120:411–437, 2013. 3

[36] Jaime Sevilla, Lennart Heim, Anson Ho, Tamay Besiroglu, Marius Hobbahn, and Pablo Villalobos. Compute trends across three eras of machine learning. In *2022 International Joint Conference on Neural Networks (IJCNN)*, 2022. 3

[37] Robert S Siegler and Zhe Chen. Developmental differences in rule learning: A microgenetic analysis. *Cognitive Psychology*, 36(3):273–310, 1998. 3

[38] Kevin Smith, Lingjie Mei, Shunyu Yao, Jiajun Wu, Elizabeth Spelke, Josh Tenenbaum, and Tomer Ullman. Modeling expectation violation in intuitive physics with coarse probabilistic object representations. *Advances in neural information processing systems*, 32, 2019. 3

[39] Kevin A Smith and Edward Vul. Sources of uncertainty in intuitive physics. *Topics in cognitive science*, 5(1):185–199, 2013. 3

[40] Kevin A Smith, Jessica B Hamrick, Adam N Sanborn, Peter W Battaglia, Tobias Gerstenberg, Tomer D Ullman, and Joshua B Tenenbaum. Probabilistic models of physical reasoning. *Reverse engineering the mind: Probabilistic models of cognition*, 2024.

[41] Felix A Sosa, Tomer Ullman, Joshua B Tenenbaum, Samuel J Gershman, and Tobias Gerstenberg. Moral dynamics: Grounding moral judgment in intuitive physics and intuitive psychology. *Cognition*, 217:104890, 2021. 3

[42] Elizabeth Spelke. *What babies know: Core knowledge and composition volume 1*. Oxford University Press, 2022. 2

[43] Elizabeth S. Spelke. Principles of object perception. *Cognitive Science*, 14(1):29–56, 1990. 1

[44] Elizabeth S Spelke and Katherine D Kinzler. Core knowledge. *Developmental science*, 10(1):89–96, 2007. 2

[45] JR Tresilian. Perceptual and cognitive processes in time-to-contact estimation: Analysis of prediction-motion and relative judgment tasks. *Perception & Psychophysics*, 57(2): 231–245, 1995. 3

[46] Tomer D Ullman, Elizabeth Spelke, Peter Battaglia, and Joshua B Tenenbaum. Mind games: Game engines as an architecture for intuitive physics. *Trends in cognitive sciences*, 21(9):649–665, 2017. 1, 3

[47] YingQiao Wang and Tomer D Ullman. Resource bounds on mental simulations: Evidence from a liquid-reasoning task. *Journal of Experimental Psychology: General*, 2025. 3

[48] Justin N Wood, Tomer D Ullman, Brian W Wood, Elizabeth S Spelke, and Samantha MW Wood. Object permanence in newborn chicks is robust against opposing evidence. *arXiv preprint arXiv:2402.14641*, 2024. 2

[49] Enze Xie, Wenhui Wang, Zhiding Yu, Anima Anandkumar, Jose M. Alvarez, and Ping Luo. Segformer: Simple and efficient design for semantic segmentation with transformers. In *Advances in Neural Information Processing Systems (NeurIPS)*, 2021. 3

[50] Bolei Zhou, Hang Zhao, Xavier Puig, Sanja Fidler, Adela Barriuso, and Antonio Torralba. Scene parsing through ade20k dataset. In *Proceedings of the IEEE Conference on Computer Vision and Pattern Recognition (CVPR)*, pages 5122–5130. IEEE, 2017. 4